

# UC San Diego

## UC San Diego Previously Published Works

### Title

Corrigendum to "Short-lived increase in erosion during the African Humid Period: Evidence from the northern Kenya Rift" [Earth Planet. Sci. Lett. 459 (2017) 58-69]

### Permalink

<https://escholarship.org/uc/item/4w37r21b>

### Authors

Garcin, Yannick  
Schildgen, Taylor F  
Acosta, Verónica Torres  
et al.

### Publication Date

2017-09-01

### DOI

10.1016/j.epsl.2017.07.027

Peer reviewed



## Short-lived increase in erosion during the African Humid Period: Evidence from the northern Kenya Rift



Yannick Garcin<sup>a,\*</sup>, Taylor F. Schildgen<sup>a,b</sup>, Verónica Torres Acosta<sup>a</sup>, Daniel Melnick<sup>a,c</sup>, Julien Guillemoteau<sup>a</sup>, Jane Willenbring<sup>b,d</sup>, Manfred R. Strecker<sup>a</sup>

<sup>a</sup> Institut für Erd- und Umweltwissenschaften, Universität Potsdam, Germany

<sup>b</sup> Helmholtz-Zentrum Potsdam, Deutsches GeoForschungsZentrum GFZ, Telegrafenberg Potsdam, Germany

<sup>c</sup> Instituto de Ciencias de la Tierra, Universidad Austral de Chile, Casilla 567, Valdivia, Chile

<sup>d</sup> Scripps Institution of Oceanography – Earth Division, University of California, San Diego, La Jolla, USA

### ARTICLE INFO

#### Article history:

Received 2 June 2016

Received in revised form 4 November 2016

Accepted 8 November 2016

Available online 30 November 2016

Editor: A. Yin

#### Keywords:

northern Kenya Rift

Baragoi

paleo-delta

African Humid Period

erosion

<sup>10</sup>Be

### ABSTRACT

The African Humid Period (AHP) between ~15 and 5.5 cal. kyr BP caused major environmental change in East Africa, including filling of the Suguta Valley in the northern Kenya Rift with an extensive (~2150 km<sup>2</sup>), deep (~300 m) lake. Interfingering fluvio-lacustrine deposits of the Baragoi paleo-delta provide insights into the lake-level history and how erosion rates changed during this time, as revealed by delta-volume estimates and the concentration of cosmogenic <sup>10</sup>Be in fluvial sand. Erosion rates derived from delta-volume estimates range from 0.019 to 0.03 mm yr<sup>-1</sup>. <sup>10</sup>Be-derived paleo-erosion rates at ~11.8 cal. kyr BP ranged from 0.035 to 0.086 mm yr<sup>-1</sup>, and were 2.7 to 6.6 times faster than at present. In contrast, at ~8.7 cal. kyr BP, erosion rates were only 1.8 times faster than at present. Because <sup>10</sup>Be-derived erosion rates integrate over several millennia, we modeled the erosion-rate history that best explains the <sup>10</sup>Be data using established non-linear equations that describe *in situ* cosmogenic isotope production and decay. Two models with different temporal constraints (15–6.7 and 12–6.7 kyr) suggest erosion rates that were ~25 to ~300 times higher than the initial erosion rate (pre-delta formation). That pulse of high erosion rates was short (~4 kyr or less) and must have been followed by a rapid decrease in rates while climate remained humid to reach the modern <sup>10</sup>Be-based erosion rate of ~0.013 mm yr<sup>-1</sup>. Our simulations also flag the two highest <sup>10</sup>Be-derived erosion rates at ~11.8 kyr BP related to non-uniform catchment erosion. These changes in erosion rates and processes during the AHP may reflect a strong increase in precipitation, runoff, and erosivity at the arid-to-humid transition either at ~15 or ~12 cal. kyr BP, before the landscape stabilized again, possibly due to increased soil production and denser vegetation.

© 2016 Elsevier B.V. All rights reserved.

### 1. Introduction

Climate change in the tropics and subtropics associated with rapid changes in erosion, soil thickness, and vegetation cover is the focus of many recent research efforts to better understand the impact of environmental change on landscapes (e.g., Pelletier et al., 2015; Schildgen et al., 2016). Paleo-environmental changes recorded by proxy indicators in marine and terrestrial sediments may serve as powerful proxies of landscape response to both

\* Corresponding author at: Institut für Erd- und Umweltwissenschaften, Universität Potsdam, Karl-Liebknecht-Str. 24, Haus 27, 14476 Potsdam-Golm, Germany. Fax: +49 331 977 5700.

E-mail address: yannickgarcin@yahoo.fr (Y. Garcin).

present-day climate variability and future climate change (e.g., deMenocal et al., 2000; Shanahan et al., 2015). In this context, the sedimentary basins of the tropical East African Rift System may furnish valuable information on how future shifts in rainfall and vegetation will impact the environment (e.g., Wolff et al., 2011; Ivory et al., 2014).

In East Africa, environmental conditions during the African Humid Period (AHP) were dramatically different between ~15 and 5.5 cal. kyr BP: (1) pollen spectra and carbon and hydrogen isotopes measured in plant leaf-waxes document shifts in the dominance of forests/woodlands versus grasslands following shifts in rainfall (Kendall, 1969; Tierney et al., 2010); (2) lacustrine sediments record oscillating lakes with co-varying changes in water chemistry and biota, reflecting alternating wetter and drier periods (Richardson and Dussinger, 1986; Bergner et al., 2009;

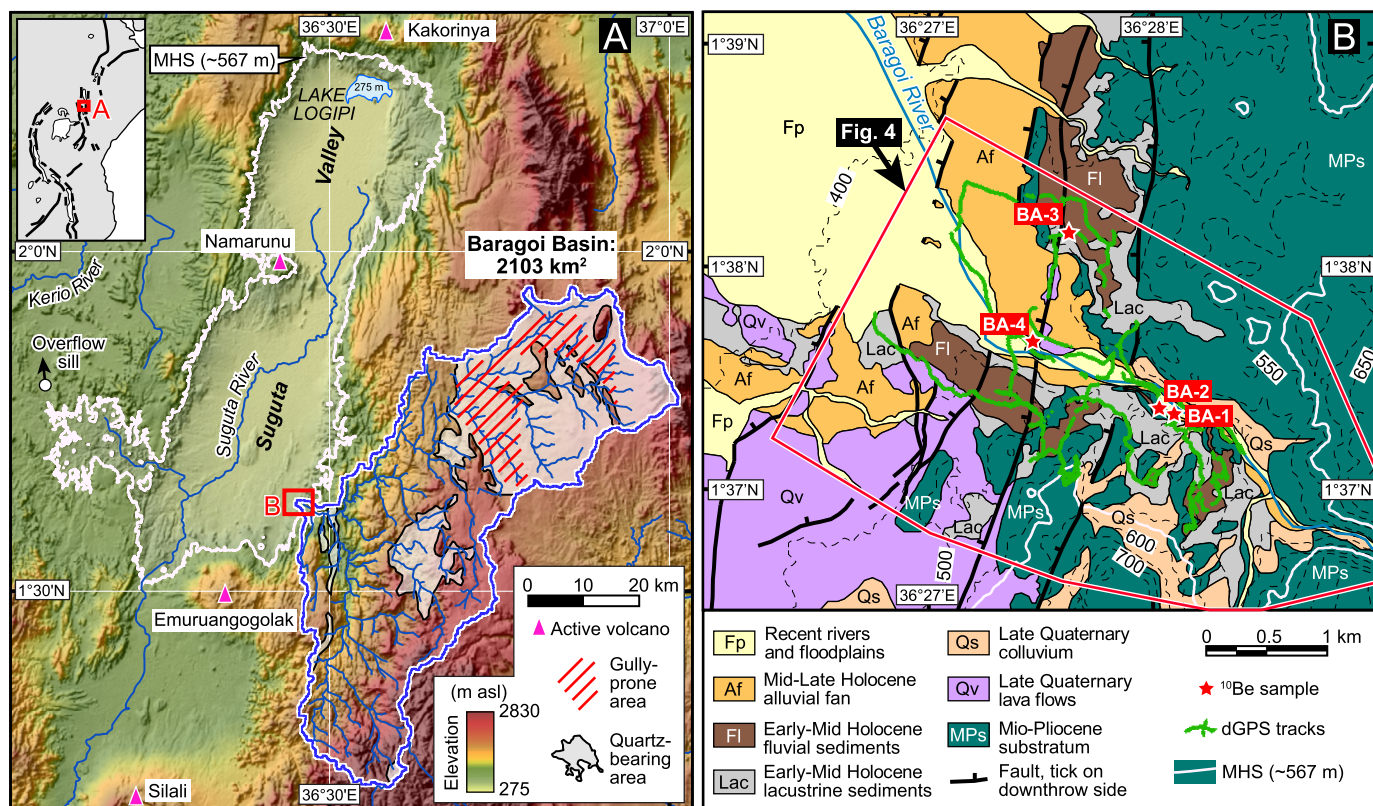


**Fig. 1.** (A) Overview of the Suguta Valley including the Baragoi drainage area. Digital elevation model based on the Shuttle Radar Topography Mission (SRTM) 90 m resolution data. Also shown is a contour at  $\sim 567$  m indicating the maximum extent of the paleo-Lake Suguta (MHS, white line; after Garcin et al., 2009), quartz-bearing areas within the Baragoi Basin, which represent 42% of the total catchment area (transparent layer; after BEICIP, 1987), and areas prone to gullying derived from the analysis of high-resolution satellite images. Inset depicts structural setting of the East African Rift System. (B) Geological and structural map of the Baragoi paleo-delta area (after Dunkley et al., 1993; this study) with locations of  $^{10}\text{Be}$  samples and dGPS tracks. Contours are at 50-m intervals. (For interpretation of the colors in this figure, the reader is referred to the web version of this article.)

Morrissey and Scholz, 2014). To date, there is only limited knowledge about past erosion in East Africa with respect to the processes, rates, and fluctuations in rainfall.

In areas that are sensitive to climate change, it has been suggested that increased rainfall and runoff may result in accelerated erosion rates (Summerfield and Hulton, 1994; Heimsath et al., 2010). However, the relationship between erosion rate and rainfall is not always straightforward. This is partly due to evapotranspiration, soil production, and vegetation cover, which may counteract expected increases in runoff and/or decrease the surface erodibility (e.g., Istanbuloglu and Bras, 2005; Vanacker et al., 2007; Molina et al., 2008; Torres Acosta et al., 2015), as well as changes in storminess, which may affect the efficiency of fluvial (Lague et al., 2005) and hillslope (Enzel et al., 2012; Antinao and McDonald, 2013) erosion.

Here, we investigate sediments, their volume, and their  $^{10}\text{Be}$  concentrations to reconstruct climate shifts and resulting changes in erosion associated with the AHP in the Suguta Valley of the northern Kenya Rift. We estimate the paleo catchment-mean erosion rate from the reconstruction of the original sediment volume in the Baragoi paleo-delta at the southeastern margin of the valley and compare it with estimates of present-day and paleo catchment-mean erosion rates based on cosmogenic  $^{10}\text{Be}$  concentrations in river sands and in late Pleistocene to Holocene deltaic sediments sampled at the mouth of the Baragoi River (Fig. 1). We evaluate both erosion-rate estimates in the context of our revised interpretation of the lake-level history for paleo-Lake Suguta to show how millennial-scale climate variability may impact erosional processes.

## 2. Geology and climate of the northern Kenya Rift

Cenozoic normal faulting and rift-shoulder uplift in the Kenya Rift have created pronounced relief contrasts between the flanks and basins along the volcano-tectonic axis of the rift. The sedimentary fills record the erosional history of the rift shoulders and integrate the complex relationships between tectonics and changing climatic and depositional characteristics (Dunkley et al., 1993).

The endorheic Suguta Valley is bordered by a major normal fault on the west and an antithetically faulted monocline on the east, involving multiple escarpments cut into Quaternary volcanic and sedimentary sequences (Baker, 1963; Dunkley et al., 1993). To the north and south, the Suguta Basin is bounded by the Quaternary Barrier eruptive center and Emuruangogolak volcano, respectively (Fig. 1A). The eastern flanks of the Suguta Valley mainly comprise phonolitic and basaltic volcanic flows intercalated with trachytes, pyroclastics, and sediments (Dunkley et al., 1993). These units cover a late Proterozoic gneissic basement exposed on the rift shoulder of the upper Baragoi catchment to the east ( $\sim 1700$  m asl). Quartz-bearing units cover  $877$  km $^2$  of the total  $2103$  km $^2$  Baragoi catchment area.

In Kenya, moisture transport and precipitation associated with the Intertropical Convergence Zone and the Congo Air Boundary are modulated by the East African Plateau, the rift shoulders, and high evapotranspiration (Nicholson, 1996; Bergner et al., 2009). The Suguta Valley is one of the driest regions of Kenya, with  $300$  to  $500$  mm yr $^{-1}$  precipitation, ephemeral runoff (Ojany and Ogenoo, 1973), and sparse vegetation. Under the present-day conditions,

only the northernmost part of the Suguta Valley remains covered by shallow Lake Logipi at ~275 m elevation, the base level for the ephemeral Baragoi River.

During the AHP, paleo-Lake Suguta rose more than 300 m and overflowed into Lake Turkana (Truckle, 1976; Dunkley et al., 1993; Garcin et al., 2009; Junginger et al., 2014). The late Pleistocene–early Holocene lake-level changes in the Suguta Valley triggered the accumulation of voluminous delta deposits (Figs. 1 and 2). At the end of the AHP, numerous regressive shorelines began recording the shrinking of paleo-Lake Suguta and the return to present-day conditions.

The Baragoi River enters the Suguta Valley through deeply incised volcanics and fluvio-lacustrine sediments of the late Pleistocene–Holocene Baragoi paleo-delta (Figs. 1 and 2). The incision has carved a set of gravel-covered terraces into the sediments. The base of the delta deposits, which coincides with the present-day Baragoi main stem, is composed of coarse sand and conglomeratic gravel, intercalated with lacustrine deposits (Garcin et al., 2009; Junginger et al., 2014).

### 3. Methods

#### 3.1. Field mapping

We mapped geological units and faults in the area where the Baragoi enters the Suguta Valley (Fig. 1B) and carried out topographic surveys using a dGPS (Leica GPS 1200) following the approach used in Garcin et al. (2009) and Melnick et al. (2012). We focused on sections located north and south of the river, where deltaic and lacustrine strata are well exposed (Figs. 2 and 3).

#### 3.2. $^{14}\text{C}$ chronology and lake-reservoir age

These strata were dated using seven accelerator mass spectrometry (AMS)  $^{14}\text{C}$  dates obtained from charcoal ( $n = 3$ ) and fossil carbonate shells of freshwater organisms ( $n = 4$ ), together with seven AMS  $^{14}\text{C}$  ages mostly based on charcoal dated by Junginger et al. (2014) (cf. section BG08) and one AMS  $^{14}\text{C}$  age on freshwater mollusk shells collected from the local maximum highstand shoreline of Lake Suguta (Garcin et al., 2009).  $^{14}\text{C}$ -analyses were carried out at the Kiel University and Poznań Radiocarbon laboratories. Dates were calibrated with the Oxcal 4.2 program (Bronk Ramsey, 2001) and IntCal13 curve (Reimer et al., 2013), and reported in cal. yr BP and in cal. kyr BP (calendar year and kilo year before Year 1950, respectively). Using four paired charcoal/carbonate shells collected in various lacustrine sedimentary sections across the Suguta Valley, Junginger et al. (2014) demonstrated that a lake-reservoir age affects the radiocarbon age of biogenic carbonates. They used a mean reservoir age of 1900 yr to correct all carbonate-sample ages. We note that the pooled value of the four reservoir ages is of 1930 yr. The associated errors are large (275 yr at the  $1-\sigma$  level), suggesting that the lake-reservoir age was not constant through time. Here, we used the four reservoir ages and interpolated them with the nearest neighbor algorithm to correct all carbonate-sample ages prior to calibration.

#### 3.3. Baragoi paleo-delta volume estimates

To derive one estimate of paleo-erosion rates, we reconstructed the volume of the dated deltaic deposits (Fig. 4). First, we created a 15-m DEM from ASTER imagery and dGPS ground control points using the DEM extraction module in the ENVI software (Fig. 4A). Then, we created a topographic model of the unconformity surface at the base of the paleo-delta fill by interpolating the elevation of bedrock outcrops obtained from the intersection of the DEM and pre-Quaternary bedrock from the detailed geologic map (Fig. 4B).

Fortunately, the Baragoi River exposes Miocene bedrock on most of its bed east of sampling site BA-4 (Fig. 1B), allowing for good control of the maximum thickness of the delta deposits in the eastern sector. As the gorge opens towards the west, sediments cover the bedrock. There, its depth is unconstrained, and has been inferred by extrapolating the Baragoi longitudinal profile. Next, we reconstructed the depositional surface of the paleo-delta before the onset of river incision by linear interpolation of the uppermost sediments exposed on the top surface (Fig. 4C). The volume of deltaic sediments was estimated by subtracting the bedrock from the topmost envelope surface (Fig. 4D). To estimate a catchment-mean erosion rate, we assumed sediment and bedrock densities of 2.2 and 2.8  $\text{g cm}^{-3}$ , respectively, and used the entire area of the catchment as a source of sediment, with bracketing ages from the radiocarbon chronology of the delta sediments.

#### 3.4. $^{10}\text{Be}$ analysis

##### 3.4.1. Sample collection and laboratory analysis

We determined catchment-mean modern and paleo-erosion rates by measuring the concentration of *in situ*-produced cosmogenic  $^{10}\text{Be}$  in detrital quartz sand (e.g., Bierman and Steig, 1996; Granger et al., 1996). Because  $^{10}\text{Be}$  accumulates within the upper few meters of the Earth's surface at a known rate, the concentration of  $^{10}\text{Be}$  can be related to a catchment-mean erosion rate assuming that the catchment was eroding uniformly. Although  $^{10}\text{Be}$  concentrations reflect denudation, we use the term erosion throughout to avoid switching between the two terms when referring to different approaches of determining paleo-erosion rates.

To determine  $^{10}\text{Be}$ -derived paleo-erosion rates for the Baragoi paleo-delta, we investigated an approximately 110-m-thick section of fluvial sands and conglomerates intercalated with lacustrine strata on the south side of the Baragoi. Samples BA-1 and BA-2 were collected ~5 m above the base of the section, which is located beneath ~100 m of overlying deltaic deposits. The sampling site was recently exposed by a slump after the rainy season in 2013 (Figs. 2B and 3). The ages of these samples are constrained by  $^{14}\text{C}$ -dated charcoal collected ~40 cm above the sands. Both sampled strata were conformable. In addition, we sampled charcoal and freshwater mollusk shells (*Melanooides tuberculata*) in the overlying lacustrine strata (Table 1) to further assess the relationships between changing lake levels and delta deposition.

A second section north of the Baragoi River (Figs. 1B and 2) with a quartzitic sand lens within lacustrine strata was selected for  $^{10}\text{Be}$  analysis (sample BA-3). The strata from this site are well correlated with a nearby stratigraphic column (cf. BG08) of Junginger et al. (2014). This section is located ~800 m to the southeast and is chronologically well constrained by  $^{14}\text{C}$ -dating of charcoal. Sample BA-3 was collected ~5 m beneath the overlying fluvial conglomerates, but due to subsequent incision, the horizon now lies 50 cm beneath a degradational terrace surface. The age of this sample was estimated by pooling two  $^{14}\text{C}$  ages of charcoal and freshwater-mollusk shells collected in the correlative strata of the two other sections (Fig. 2B).

In addition, we collected fluvial sands at the outlet of the Baragoi catchment (Figs. 1B and 2C) to determine the modern catchment-mean erosion rate (sample BA-4).

Sample preparation for  $^{10}\text{Be}$  analysis was performed at the GFZ Potsdam and followed standard procedures (Kohl and Nishiizumi, 1992).  $^{10}\text{Be}$  was extracted from quartz using standard methods (von Blanckenburg et al., 2004).  $^{10}\text{Be}/^9\text{Be}$  ratios were measured in BeO targets prepared by evaporating and oxidizing Be together with  $\text{AgNO}_3$ . Approximately 200  $\mu\text{g}$  of  $^9\text{Be}$  carrier were added to each sample and to blank measurements. AMS analyses were performed at ETH Zurich, at CAMS Lawrence Livermore National Laboratory, and at the University of Cologne. We relied on the original



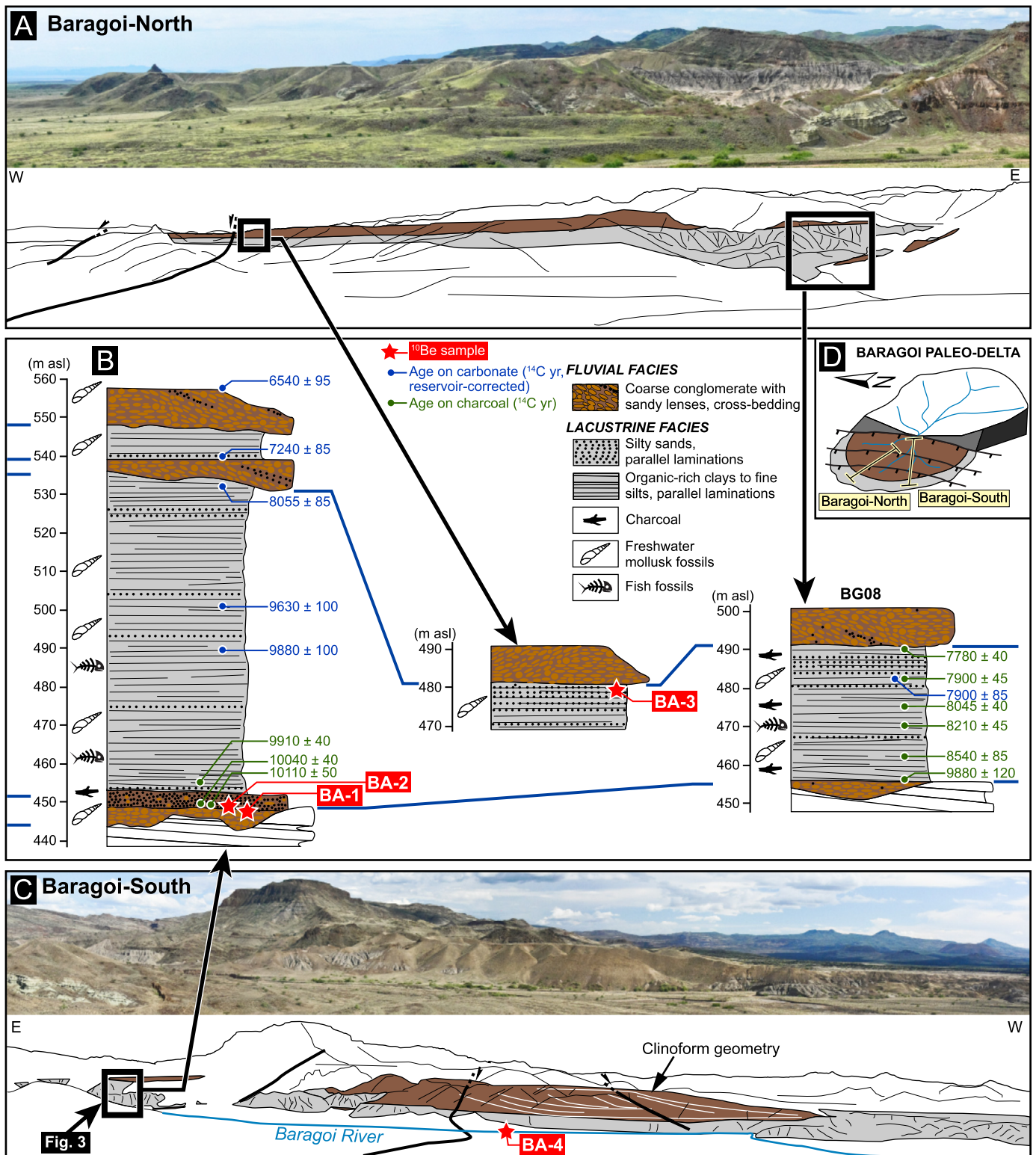


**Fig. 2.** Views of Baragoi paleo-delta. (A) Outcrops north of Baragoi River. Panorama (top) and interpretation of depositional environment (bottom). Faults are also shown. (B) Stratigraphic columns with interpretation of sedimentary environments and correlations along and across the Baragoi River mouth. Also shown are <sup>10</sup>Be samples and radiocarbon ages derived from freshwater mollusk shells and charcoal. Radiocarbon ages on stratigraphic column on far right are from Junginger et al. (2014); cf. section BG08. Highest radiocarbon age from stratigraphic column on far left is from Garcin et al. (2009). (C) As (A), but for outcrops south of the Baragoi. (D) Synthetic diagram of the Baragoi paleo-delta showing locations of outcrops. Depositional sketches in (A) and (C) are color-coded to the geologic map in Fig. 1B; stratigraphic columns (B) have their own, independent legend. (For interpretation of the references to color in this figure legend, the reader is referred to the web version of this article.)

ICN standard (07KNSTD, 07KNSTD3110, and BEST433) as reference and used a value of  $5.0 \cdot 10^{-7} \text{ yr}^{-1}$  for the decay constant for <sup>10</sup>Be (Chmeleff et al., 2010), which is equivalent to the <sup>10</sup>Be half-life of

$1.387 \pm 0.012 \text{ Myr}$  (Korschinek et al., 2010). Procedure blanks were determined to contain a <sup>10</sup>Be/<sup>9</sup>Be ratio of  $4 \pm 0.4 \cdot 10^{-15}$ , which represented <10% of the AMS ratio in the samples.

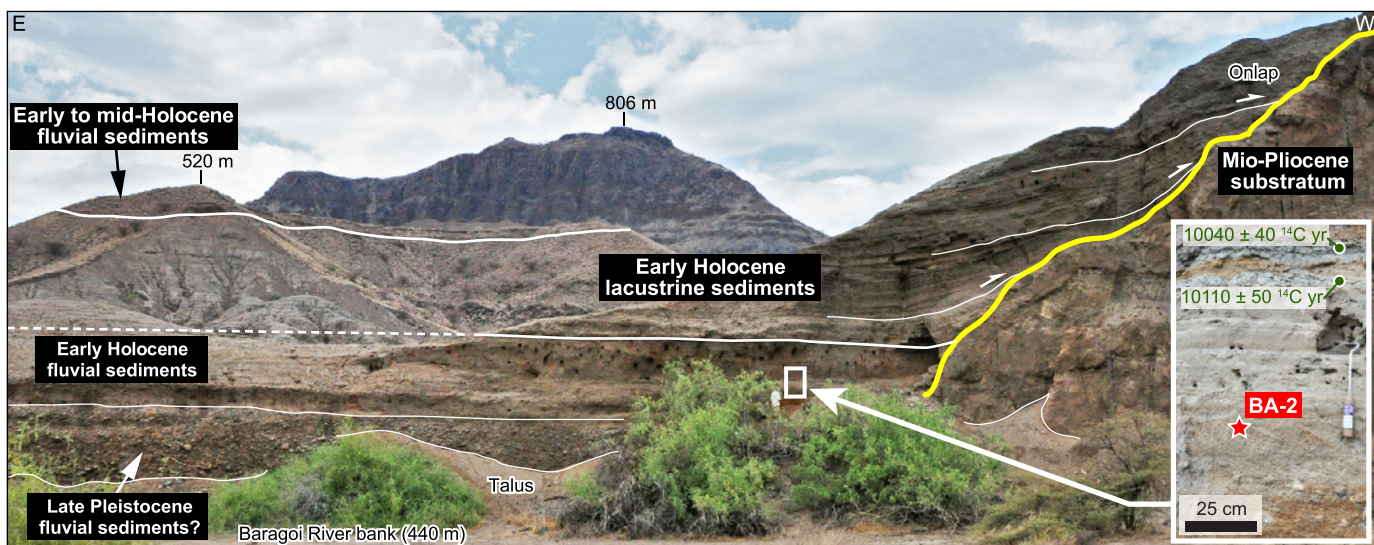


**Fig. 3.** Baragoi paleo-delta exposing alternating fluvial and lacustrine deposits, view toward south. Fluvial deposits at base of section were sampled for  $^{10}\text{Be}$  paleo-erosion rate (red star; sample BA-2); green dots denote two collected charcoal samples. Note well-developed onlap of lacustrine sediments on paleo-topography; person for scale. (For interpretation of the references to color in this figure legend, the reader is referred to the web version of this article.)

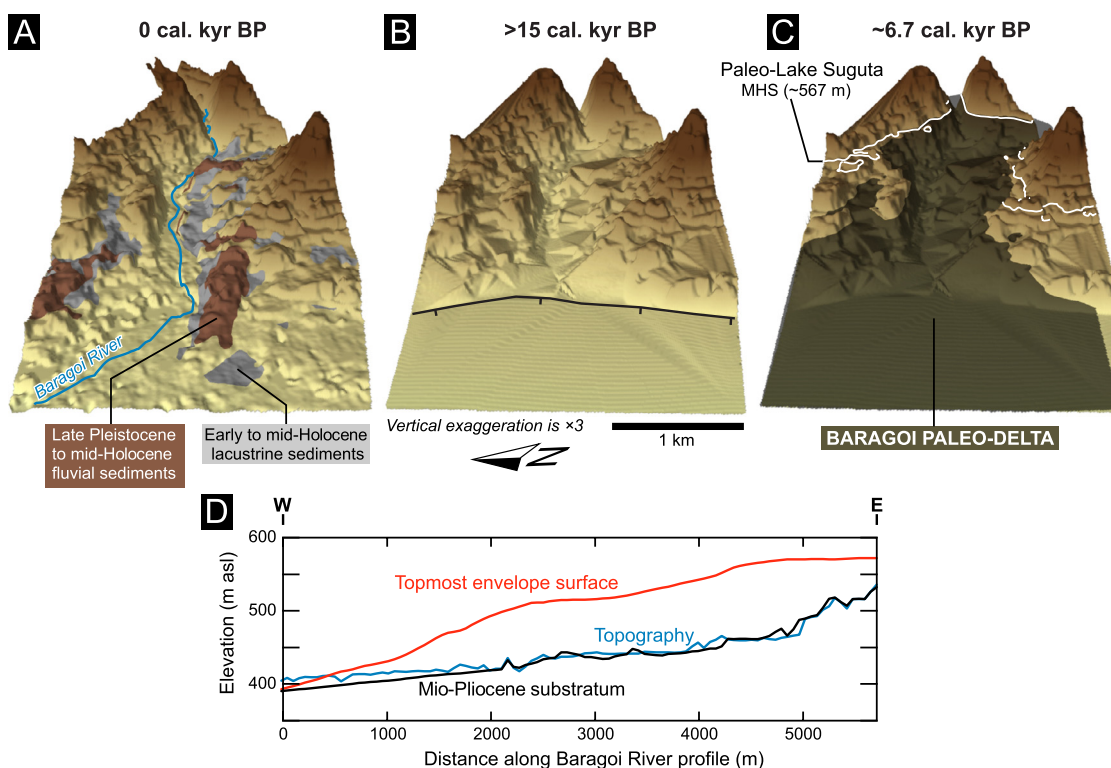


**Fig. 4.** Three-D surfaces documenting the evolution of the Baragoi paleo-delta. (A) Modern remnants of the Baragoi paleo-delta deposits. Also shown is the Baragoi River. (B) Pre-delta topography. (C) Maximum development of the Baragoi paleo-delta (dark transparent layer) during the African Humid Period. Also shown is a contour at  $\sim 567$  m indicating the maximum extent of the paleo-Lake Suguta (MHS). (D) Modern Baragoi River profile shown with the inferred Mio-Pliocene substratum and the reconstructed topmost envelope surface of the paleo-delta. (For interpretation of the colors in this figure, the reader is referred to the web version of this article.)

The catchment mean  $^{10}\text{Be}$  production rate was determined for the quartz-bearing areas of the Baragoi catchment (Fig. 1A), based on the SRTM 3 arc-second elevation data and including changes in altitude, latitude, spallation, muon production and topographic shielding. Modern and paleo-erosion rates were calculated following Balco et al. (2008) and using the Cronus calculator (V2.2; <http://hess.ess.washington.edu>).

To calculate paleo-erosion rates from the concentration of  $^{10}\text{Be}$  in the sandy facies of the deltaic strata, we must consider how

post-depositional production and decay of cosmogenic  $^{10}\text{Be}$  has altered the initial  $^{10}\text{Be}$  concentration at the time of deposition (e.g., Schaller et al., 2002). Due to the young age of the sampled deposits ( $<12$  cal. kyr BP), decay of  $^{10}\text{Be}$ , which has a half-life of  $\sim 1.4$  Myr (Korschinek et al., 2010), is insignificant. In terms of post-depositional production, rapid sediment deposition at the sites ( $\sim 25$   $\text{m yr}^{-1}$  based on the dated stratigraphy) coupled with shielding from the lake water minimizes significant nuclide accumulation during burial. Subsequent incision into the



**Table 1**  
Radiocarbon ages from the Baragoi paleo-delta.

Sample ID	Material <sup>a</sup>	Sample elevation (masl)	Lat. (°N)	Lon. (°E)	AMS <sup>14</sup> C age (yr BP) ±1-σ	Reservoir age ( <sup>14</sup> C yr) ±1-σ <sup>b</sup>	AMS <sup>14</sup> C age reservoir-corrected (yr BP) ±1-σ	Median cal. age (yr BP) <sup>c</sup>	Cal. age range (yr BP; 99.7%) <sup>c</sup>
KIA36867	L.ca	540.1	1.616891	34.469965	9210 ± 50	1970 ± 70	7240 ± 85	8070	7830/8350
KIA36868	L.ca	532.1	1.616917	36.470042	10,295 ± 55	2240 ± 65	8055 ± 85	8930	8590/9400
KIA36869	L.ca	501.2	1.617596	36.470158	11,200 ± 60	1570 ± 80	9630 ± 100	10960	10,565/11,310
KIA36870	L.ca	489.7	1.618040	36.470141	11,450 ± 60	1570 ± 80	9880 ± 100	11345	10,790/11,995
KIA42911	L.ch	455.1	1.621550	36.467200	9910 ± 40			11300	11,205/11,610
Poz-58072	F.ch	449.6	1.621704	36.467573	10,040 ± 40			11540	11,270/11,960
Poz-58073	F.ch	449.4	1.621704	36.467573	10,110 ± 50			11725	11,330/12,055

<sup>a</sup> L.ca = carbonate from lacustrine nearshore/offshore deposits; L.ch = charcoal from lacustrine nearshore/offshore deposits; F.ch = charcoal from fluvial deposits.

<sup>b</sup> Time-dependent radiocarbon reservoir age (see Fig. 5C) derived from paired charcoal/carbonate mollusk shell from the Suguta Valley (raw data: Junginger et al., 2014) and used to correct carbonate ages.

<sup>c</sup> Calibrated radiocarbon ages given before 1950; <sup>14</sup>C calibration method: program OxCal 4.2 (Bronk Ramsey, 2001) with the IntCal13 curve (Reimer et al., 2013).

strata has also likely resulted in minimal post-depositional production. For samples BA-1 and BA-2, very recent exposure following a slump minimizes the possibility of post-depositional <sup>10</sup>Be accumulation. For sample BA-3, post-depositional accumulation is expected to be only on the order of 10% the surface production rate (~3.6 atoms g<sup>-1</sup> yr<sup>-1</sup>) due to shielding from the material above the sample site. Although a precise exposure age of the terrace gravels overlying this sample is needed to properly calculate <sup>10</sup>Be accumulation since incision, the total amount is likely to be very low. We thus proceed with paleo-erosion rate calculations assuming no post-depositional accumulation. If this assumption were incorrect, our reported paleo-erosion rates would still represent minimum rates.

#### 3.4.2. Modeling <sup>10</sup>Be data

<sup>10</sup>Be is produced within the upper few meters of the Earth's surface through the interaction of secondary cosmic rays with target minerals (Lal, 1991). The concentration of <sup>10</sup>Be in detrital quartz can in turn be used to determine catchment mean-erosion rates if the catchment is being eroded uniformly and steadily, with higher concentrations corresponding to slower rates (e.g., Bierman and Steig, 1996; Granger et al., 1996). These erosion rates average over a timescale that is approximately equal to the time to exhume a thickness of rock equal to the absorption mean path length of the secondary cosmic rays, which is typically 60 to 100 cm in bedrock (Granger et al., 1996; von Blanckenburg, 2005). As such, the rates average over a shorter timescale in rapidly eroding areas compared to slowly eroding areas. This averaging timescale is important to consider when interpreting how well cosmogenic-derived erosion rates may reflect changes in erosion rates through time, particularly if a change in erosion rates occurred in the recent past.

We modeled how erosion rates derived from <sup>10</sup>Be surface concentrations change as a function of imposed changes in erosion rates to better understand how our <sup>10</sup>Be data relate to a real erosion-rate history. A Matlab<sup>®</sup> code for plotting the simulations of the models presented in this study is available at the github repository ([https://github.com/ygarcin/EPSSL\\_2017](https://github.com/ygarcin/EPSSL_2017)). We initialized our model by assuming that the landscape has experienced a uniform, steady erosion rate for long enough that the concentration of <sup>10</sup>Be with depth below the surface is unchanging (Lal, 1991),

$$N(z) = \frac{P(0)e^{-\mu z}}{\mu\epsilon + \lambda} \quad (1)$$

where  $N$  is the concentration of nuclides (atoms g<sup>-1</sup>) at depth  $z$  (cm),  $P(0)$  is the production rate of nuclides at the surface (g atoms<sup>-1</sup> yr<sup>-1</sup>),  $\mu$  is equal to the quotient of the density of denuding material ( $\rho$ , g cm<sup>-3</sup>) divided by the absorption mean path ( $\Lambda$ , g cm<sup>-2</sup>),  $\epsilon$  is the erosion rate (cm yr<sup>-1</sup>), and  $\lambda$  is the nuclide decay constant (yr<sup>-1</sup>). In subsequent time steps, the model

tracks the change in nuclide concentrations as material is advected upwards due to erosion. The concentrations evolve over time according to the relationship described by Lal (1991):

$$\frac{dN(z)}{dt} = -N(z)\lambda + P(0)e^{-\mu z} \quad (2)$$

We calculated concentrations in depth increments of 2 mm, with time steps equal to the time required to remove 2 mm of material from the surface. Because we explored a range of erosion rates between 0.005 and 1.6 mm yr<sup>-1</sup>, our time steps ranged from 400 to 1.25 yr. The initial depth to which we calculate concentrations is based on the total depth of material exhumed through the model simulation. We assumed a density of 2.7 g cm<sup>-3</sup> of denuding bedrock and an attenuation length of 160 g cm<sup>-2</sup> for neutron spallation. We did not include muogenic <sup>10</sup>Be production in our model; including it would lead to a change in our calculated erosion rates of a few percent, but this is well within the typical ~10 to 20% uncertainty in erosion rates calculated from <sup>10</sup>Be concentrations. Following an imposed erosion-rate history, the model calculates the predicted <sup>10</sup>Be-derived erosion rates through time based on changes in the surface concentration of <sup>10</sup>Be, which is determined by solving for  $\epsilon$  at  $z=0$  in eq. (1):

$$\epsilon = \frac{P(0) - N(0)\lambda}{N(0)\mu} \quad (3)$$

where  $N(0)$  is the nuclide concentration at the surface.

## 4. Results

### 4.1. Stratigraphy and chronology of the Baragoi paleo-delta

The incised vestiges of the Baragoi paleo-delta, which was at least 10 km long and 7 km wide (Figs. 1B and 4), are found north and south of where the Baragoi enters the Suguta Valley. Cemented conglomerates at the top armor the underlying lacustrine silts and help preserve them.

The oldest sediments of the paleo-delta are coarse conglomerates that were deposited atop a bedrock unconformity sculpted into Mio-Pliocene rocks (Figs. 2B and 3). The conglomerates are five meters thick and comprise well-rounded clasts with a sandy matrix. These strata are superseded by cross-bedded coarse sands with cobbles, medium, parallel-stratified sands, organic-rich silty clays containing charcoal fragments, and finally cross-bedded coarse sands and fine to medium conglomerates. We interpret this fining-upward section to have been associated with fluvial processes during a rising base level, and ensuing filling of fluvial channels in the lowest sectors of the rift. The age of the basal conglomerate is unknown, but the overlying organic-rich silty clays provided ages between 11,725 and 11,540 cal. yr BP (Table 1).

The fluvial sediments are overlain by ~40 to ~80 m of monotonous, unconsolidated, laminated clayey to silty deposits; they contain abundant freshwater mollusk shells (*Melanoides tuberculata*), fish bones, and occasionally charcoal. These units reflect continuous lacustrine conditions, which existed during a protracted lake highstand.  $^{14}\text{C}$  ages sampled at the bottom and top of this lacustrine unit suggest it formed between ~11,380 and ~8750 cal. yr BP (Table 1).

Towards the top of the lacustrine unit, sandy layers are more frequent, and there is an increase in grain size (Junginger et al., 2014), which culminates with a coarse, cross-bedded fluvial conglomerate truncating the lacustrine strata. The conglomerate, which is ten meters thick in the proximal part of the paleo-delta, may reach a thickness of 60 m in its distal part, where clinoform geometry is observed (Fig. 2C). This depositional pattern indicates a phase of progradation of the Baragoi paleo-delta coupled with high sediment supply and limited accommodation space. A layer of lacustrine sediments similar to the lower unit is intercalated with the topmost conglomerate unit of the most proximal stratigraphic section (Fig. 2B). The brief return of lacustrine conditions suggests a local increase in accommodation space, possibly associated with fault-induced subsidence driven by ongoing extension (Melnick et al., 2012). The deposition of the main fluvial unit during delta progradation occurred between ~8.7 and 6.7 cal. kyr BP; the latter is the youngest age of the maximum highstand shoreline of the paleo-lake (Garcin et al., 2009).

#### 4.2. Volume of the Baragoi paleo-delta and catchment-mean erosion rates

The total volume of the Baragoi paleo-delta sediments estimated by subtracting the bedrock surface from the top envelope surface is  $0.43 \text{ km}^3$ ; this is equivalent to  $0.33 \text{ km}^3$  of the predominantly volcanic rocks eroded from the entire catchment. The catchment area of  $2103 \text{ km}^2$  combined with the oldest and youngest ages of 12 and 6.7 cal. kyr BP yields a catchment-mean erosion rate of  $0.03 \text{ mm yr}^{-1}$  (Fig. 5A). Alternatively, if we assume that the deposition of the delta sediments occurred between 15 and 6.7 cal. kyr BP, which includes the first lake highstand (Fig. 5D) during the early AHP in the Suguta Valley, the catchment-mean erosion rate would be  $0.019 \text{ mm yr}^{-1}$ .

#### 4.3. $^{10}\text{Be}$ catchment-mean erosion rates

Our  $^{10}\text{Be}$  analyses from the paleo-delta sediments yielded paleo catchment-mean erosion rates of  $0.035 \pm 0.003$ ,  $0.086 \pm 0.006$ , and  $0.024 \pm 0.002 \text{ mm yr}^{-1}$  for samples BA-1, BA-2, and BA-3, respectively (Table 2). The sand sample collected from the present-day river (BA-4) yielded a modern catchment-mean erosion rate of  $0.013 \pm 0.001 \text{ mm yr}^{-1}$ . The early Holocene  $^{10}\text{Be}$ -derived erosion rates are thus 1.8 to 6.6 times higher than the modern rate. This is comparable to the rates based on the volumetric calculation of the delta deposits if the highest  $^{10}\text{Be}$ -derived erosion rate is omitted (Fig. 5A). These values are consistent with a recently published dataset of catchment-mean  $^{10}\text{Be}$  erosion rates in East Africa, which range from 0.015 to  $0.15 \text{ mm yr}^{-1}$  for a wide range of climate zones and hillslope gradients (Torres Acosta et al., 2015). However, the  $^{10}\text{Be}$  erosion rates are only representative of the upper parts of the catchment that exposes gneisses on polycyclic erosion surface at elevations of ~1100–2200 m. This area could generate slower erosion rates compared to the rest of the catchment due to its lower slopes, but it is difficult to test this without collecting samples from different locations. Although this may complicate comparisons of the  $^{10}\text{Be}$ -derived erosion rates to those derived from the deltaic sediments, they do not affect our

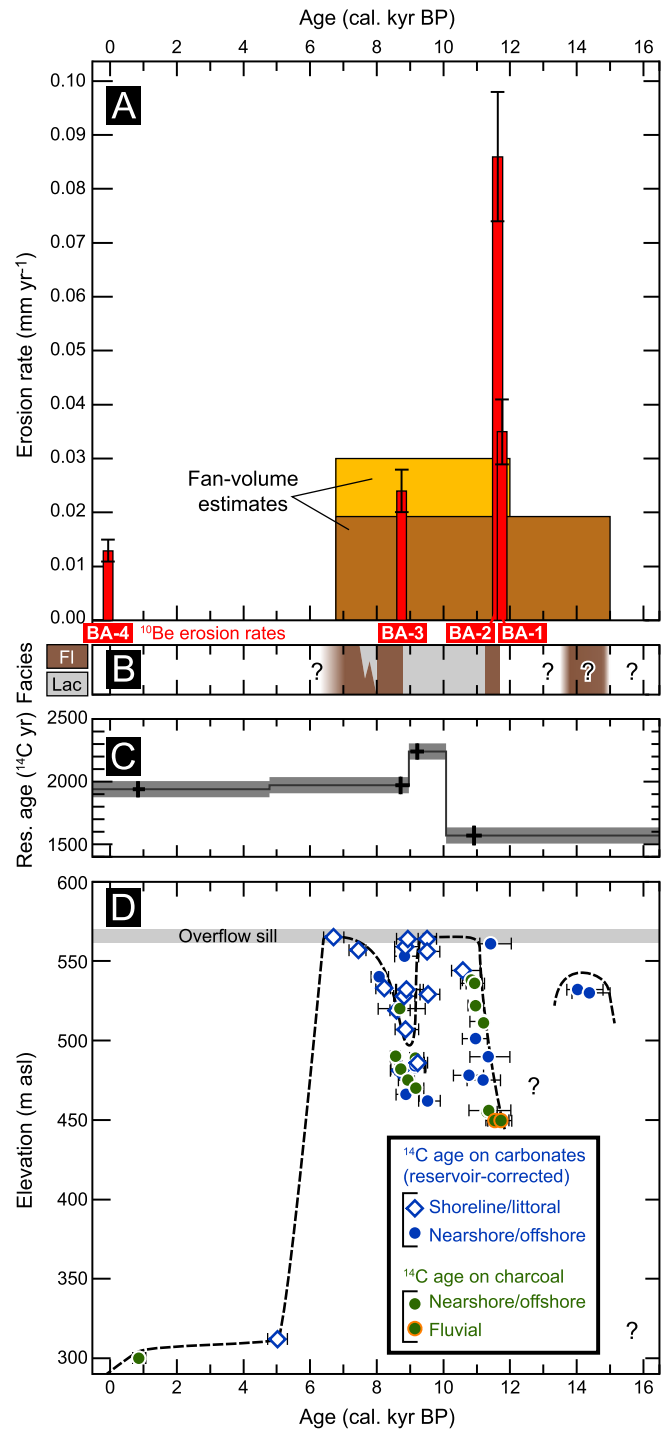


**Fig. 5.** Comparison of erosion rates measured in the area of the Baragoi River mouth with lake-level reconstruction of the paleo-Lake Suguta during the last 15 cal. kyr BP. (A) Erosion rates derived from  $^{10}\text{Be}$  concentration (red bars, sample names are shown below) and from delta-volume estimate (brown surface ranges from 15 to 6.7 kyr BP; orange surface ranges from 12 to 6.7 kyr BP). Uncertainties are shown at the 2- $\sigma$  level. (B) Main facies of Baragoi paleo-delta: Fl = fluvial facies; Lac = lacustrine facies. (C) Paleo-Lake Suguta radiocarbon reservoir-age record based on paired charcoal/carbonate mollusk shells. Raw data from Junginger et al. (2014) and nearest neighbor interpolation (grey surface, 1- $\sigma$  level). (D) Reassessed lake-level curve of paleo-Lake Suguta (dashed line) based on this study and previously published data (Garcin et al., 2009; Junginger et al., 2014). Lake-level curve is a compilation of dated fluvial deposits and lacustrine deposits reflecting shoreline to offshore environments. Radiocarbon ages on carbonates were corrected for old carbon using a variable reservoir age shown in (C). Calendar age uncertainties are shown with a probability interval of 99.7%. (For interpretation of the references to color in this figure legend, the reader is referred to the web version of this article.)



**Table 2**  
Cosmogenic nuclide analytical data for samples from the area of the Baragoi River mouth.

Sample	Sample elevation (m asl)	Latitude (°N)	Longitude (°E)	Estimated age (cal. yr BP)	$^{10}\text{Be}$ atoms ( $10^3$ atoms $\text{g}_{\text{qtz}}^{-1}$ )	$^{10}\text{Be}$ atoms uncertainty, $1-\sigma$ ( $10^3$ atoms $\text{g}_{\text{qtz}}^{-1}$ )	Erosion rate ( $\text{mm yr}^{-1}$ )	Erosion rate uncertainty ( $1-\sigma$ ) ( $\text{mm yr}^{-1}$ )	Integration time (kyr)
<i>Modern river sands</i>									
BA-4	426	1.62726	36.45776	~60	18.8	0.3	0.013	0.001	46
<i>Early Holocene fluvial sands</i>									
BA-3	479	1.63584	36.46012	~8745	9.9	0.2	0.024	0.002	25
BA-2	449	1.62170	36.46757	~11,750	2.8	0.2	0.086	0.006	7
BA-1	448	1.62153	36.46810	~11,750	4.4	0.2	0.035	0.003	17

<sup>a</sup> Standard used for normalization was 07KNSTD3110;  $^{10}\text{Be}/^9\text{Be}$  ratio for standard =  $2.85\text{e}^{-12}$ .

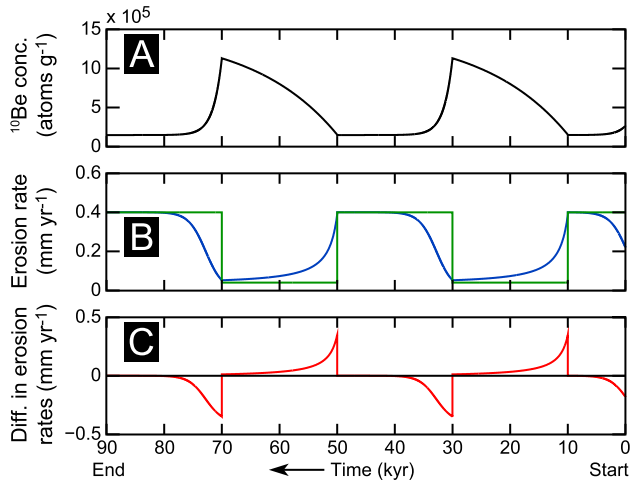


**Fig. 6.** Erosion model simulating step changes. (A) Change in  $^{10}\text{Be}$  concentration (black line). (B) Change in erosion rate derived from  $^{10}\text{Be}$  concentration (blue line) in sediment as a response of imposed real erosion (green line). (C) Difference in real and  $^{10}\text{Be}$ -derived erosion rate (red line). In our model we imposed step changes in erosion rates between 0.04 and 0.4  $\text{mm yr}^{-1}$  every 20 kyr. (For interpretation of the references to color in this figure legend, the reader is referred to the web version of this article.)

interpretation of changes in  $^{10}\text{Be}$ -derived erosion rates through time.

#### 4.4. Modeling $^{10}\text{Be}$ -derived erosion rates

We first illustrate the lag in the cosmogenic signal relative to real erosion rates by imposing step changes in erosion rates between 0.04 and 0.4  $\text{mm yr}^{-1}$  every 20 kyr in our model (Fig. 6). Following an increase in erosion rate, it takes  $\sim 7$  kyr for the  $^{10}\text{Be}$  signal to match the imposed signal. In contrast, following a decrease in erosion rate, the  $^{10}\text{Be}$  signal has still not matched the imposed signal after 20 kyr. Whereas the length of the lag in the  $^{10}\text{Be}$  signal is related to the direction and magnitude of the change, generally, the lag time associated with an increased erosion rate is shorter than that associated with a decreased erosion rate (Bierman and Steig, 1996; von Blanckenburg, 2005). This illustrates that high-frequency changes in erosion rates can result in  $^{10}\text{Be}$ -derived erosion rates that do not match real erosion rates, hence they may only be considered “apparent” erosion rates.

We next used our model to try to find an erosion-rate history that matches the apparent erosion rates calculated from our  $^{10}\text{Be}$  samples (Fig. 7). Our model was constrained by the duration of the delta formation. Because the age of the basal conglomerates, which marks the beginning of the Baragoi paleo-delta, is either  $\sim 15$  or  $\sim 12$  cal. kyr BP (see Section 5.1), we used these two ages to constrain the earliest possible start of the erosion pulse in two simulations. Although we have no estimates for erosion rates

prior to the formation of the delta, lake-levels were probably similar to the modern day or lower as observed in other sectors of the East African Rift, prior to 15 cal. kyr BP (Butzer et al., 1972; Gasse et al., 2008; Bergner et al., 2009; Morrissey and Scholz, 2014), and hydroclimate was likely similar to modern conditions. Hence, we assume that erosion rates prior the erosion pulse were similar to the modern imposed erosion rate of 0.005  $\text{mm yr}^{-1}$  (see below). During the subsequent erosion pulse, the erosion rate in both simulations was increased to between 0.1 and 1.6  $\text{mm yr}^{-1}$  (increments of 0.02  $\text{mm yr}^{-1}$ ) for a duration that lasted at most until 6.7 cal. kyr BP (increments of 100 yr), when the lake receded. The erosion rate was then kept low (at 0.005  $\text{mm yr}^{-1}$ ) and constant until the present. Within this parameter space, we generated 258,628 and 104,728 simulations for the models bounded at 15 and 12 cal. kyr BP, respectively. Only the simulations that fit the data within at least  $3-\sigma$  uncertainty were stored.

We found no erosion-rate history that predicts the erosion rates from all our samples (Fig. 7). The closest matches can be found after excluding the highest erosion rates (samples BA-1 and BA-2). Forcing the model to reach the highest value creates an erosion-rate history that cannot match the remaining samples (Electronic Annex EA-1). Exclusion of these two samples would be reasonable if an increase in erosion rates resulted in non-uniform erosion across the catchment, for example if gullies or sudden mass movements locally excavated material from deep within the hillslopes, mobilizing material with particularly low  $^{10}\text{Be}$  concentrations (e.g., Niemi et al., 2005). We note that today gullies exist in the quartz-bearing areas (Fig. 1A). After excluding these samples, we still do not find an erosion-rate history that predicts our remaining  $^{10}\text{Be}$ -derived rates within a  $2-\sigma$  uncertainty, but the range does fall within a  $3-\sigma$  uncertainty (Fig. 7).

Because we assume a relatively low erosion rate at the start of the simulations, a large, sudden increase in erosion rate is required to obtain rates similar to sample BA-3, depending on the models. The imposed erosion rates required for both investigated time periods of delta formation are  $\sim 25$  to  $\sim 300$  times higher than the initial erosion rate (depending on the erosion-step duration); ranging from 0.12 to 1.6  $\text{mm yr}^{-1}$ . That pulse of high erosion must be followed by a rapid decrease in erosion rates (of similar magnitude) to approach the lower erosion rate of sample BA-4.

## 5. Discussion

### 5.1. Fluctuations of paleo-Lake Suguta and delta formation

By combining our new ages of fluvio-lacustrine deposits of the Baragoi paleo-delta with previously published data from the Suguta Valley (Garcin et al., 2009; Junginger et al., 2014), we reassess the Suguta lake-level curve since  $\sim 15$  cal. kyr BP to evaluate the relationships between climate-driven lake-level rise and delta formation. We compiled a total of 51 radiocarbon ages (Garcin et al., 2009; Junginger et al., 2014) (Fig. 5D), which are documented in

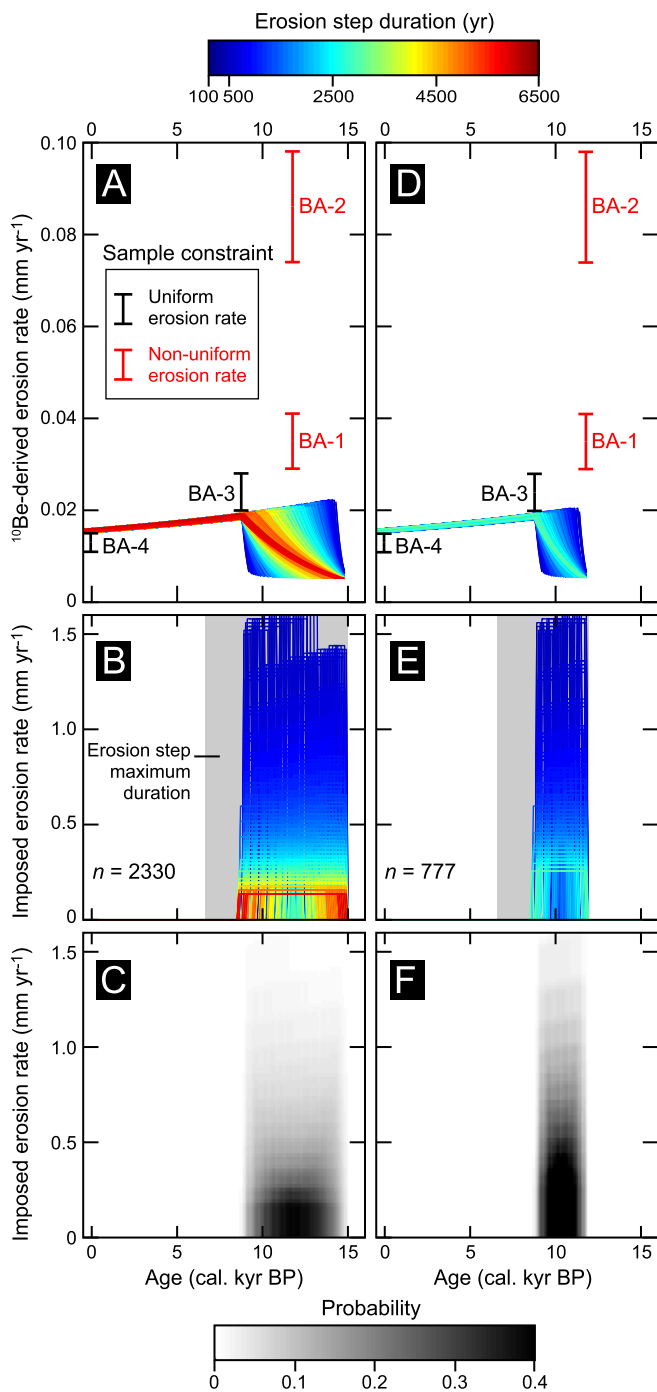


**Fig. 7.** Model simulations of erosion-rate history that best matches the erosion rates calculated from  $^{10}\text{Be}$  samples. Only simulations that fit the data within  $3\text{-}\sigma$  uncertainty are presented.  $^{10}\text{Be}$ -derived erosion history (A, D) is constrained by the data (samples BA-1–4; uncertainties are shown at the  $2\text{-}\sigma$  level) and the erosion step models (B, E); the maximum duration of the latter (gray surface) being related to the hypothesized period of delta formation.  $n$  is the number of models that fulfilled the conditions set for each scenario. Color scale shows variation in erosion step duration. Probability of each model is shown in grayscale (C, F). (A–C) Erosion step model forced between 15 and 6.7 kyr. (D–F) Erosion step model forced between 12 and 6.7 kyr. For both scenarios, samples BA-1 and BA-2 were treated as non-uniform erosion rates and excluded. (For interpretation of the references to color in this figure legend, the reader is referred to the web version of this article.)

the Electronic Annex EA-2. The ages were determined on charcoal and mollusk shells from lacustrine sediments, which formed in shoreline/littoral to nearshore/offshore environments, as well as from fluvial sediments.

Our new compilation differs from that of Junginger et al. (2014) in that it includes new ages from the Baragoi delta and a new reservoir-age correction applied to the biogenic carbonates. Junginger et al. (2014) used a constant mean reservoir age to correct all carbonate-sample ages. In contrast, we applied a variable reservoir age (see Section 3.2 and Fig. 5C). A greater number of paired charcoal/carbonate material is needed to determine a robust time-dependent reservoir age; hence, our continuous interpolation of the reservoir ages in time may be too simplistic. Nonetheless, our new reservoir-age correction on carbonates results in an apparent clustering of both carbonate and charcoal  $^{14}\text{C}$  ages for two periods, centered at  $\sim 11$  and  $\sim 9$  cal. kyr BP. Such  $^{14}\text{C}$  age clusters measured on samples of different material collected at various elevations and localities suggest an accurate radiocarbon reservoir correction (Fig. 5D). In contrast, the use of a constant reservoir-age correction (Junginger et al., 2014) resulted in a highly scattered distribution of  $^{14}\text{C}$  ages on carbonate samples. Combined with the distribution of the  $^{14}\text{C}$  ages on charcoal, this scatter was interpreted to reflect high frequency/high amplitude water-level fluctuations related to changes in solar irradiation. Our reevaluated chronology does not show such variability and instead provides the basis for a more conservative lake-level history, which is described below.

Dated lacustrine sediments in the southwesternmost part of the Suguta Valley record a highstand probably at  $\sim 15\text{--}14$  cal. kyr BP (Garcin et al., 2009; Junginger et al., 2014), coeval with the onset of the AHP (deMenocal et al., 2000). The undated basal conglomerates at Baragoi may have been either contemporaneous with this initial rise of paleo-Lake Suguta or with the second lake-level rise at  $\sim 12$  cal. kyr BP. Whereas a drop in base level is expected to result in a wave of incision that may propagate far upstream, a rise in base level should cause deposition at the channel outlet and aggradation along the fluvial network (Schumm, 1993), both of which we observe along the lower Baragoi. This interpretation of a rising base-level is supported by the nature of the conglomeratic fill, which covers an erosional paleo-landscape in the Mio-Pliocene units, with greater thicknesses attained in paleo-channels (Fig. 2). Accordingly, finer-grained facies must have been deposited in the basin center. The exact duration of the initial lake highstand is unknown. However, the absence of lacustrine sediments in the Suguta Valley between  $\sim 14$  and  $12$  cal. kyr BP suggests a lake regression of unknown magnitude (Junginger et al., 2014). Subsequently, the water level rose abruptly by at least  $100$  m between  $\sim 12$  and  $\sim 11$  cal. kyr BP, reaching its highest level of  $\sim 567$  m asl, where it may have remained until  $\sim 9.5$  cal. kyr BP. Most of the Baragoi delta sediments aggraded during this highstand. The lake level dropped  $\sim 50$  m at  $\sim 9$  cal. kyr BP, coinciding with the deposition of fluvial conglomerates. Subsequent to this intermediate, short-lived lowstand, the lake level rose again and reached its overflow level, draining into Lake Turkana. This highstand was accompanied by progradation of the coarse conglomerates of the Baragoi paleo-delta. The highstand lasted until  $\sim 6.7$  cal. kyr BP when the lake level fell to  $\sim 310$  m asl at  $\sim 5$  cal. kyr BP, finally reaching the present-day low.

## 5.2. Erosion-rate estimates and limitations

The average-erosion rate reconstructed from the volume of the Baragoi delta sediments is of  $0.019\text{ mm yr}^{-1}$  for the total duration of the paleo-Lake Suguta highstand, from  $\sim 15$  to  $\sim 6.7$  cal. kyr BP, or  $0.03\text{ mm yr}^{-1}$ , if we assume that delta deposition was only active from  $\sim 12$  to  $\sim 6.7$  cal. kyr BP. These estimates are similar to the  $^{10}\text{Be}$ -derived catchment-wide erosion rates from the paleo-delta deposits. However, the erosion rate based on the volumetric calculation is a minimum value, because most of the fine-grained sediments must have been deposited in more distal areas of the

lake basin, and any dissolved load derived from chemical weathering is not included. Also, uncertainty arises from the extrapolation of the bedrock surface west of the last exposed normal fault, highlighted in Figs. 1B and 4B. The slope of the Baragoi gorge provides a minimum dip for the bedrock surface, as it is covered by sediments, leading to an underestimation of the sediment volume.

Our observations show that the Baragoi paleo-delta was constructed during a lake highstand, when ample accommodation space existed in the basin. If a pulse of high erosion occurred prior to the lake highstand, the sediment would not have been deposited in the same location as the delta, and would not be recorded in the volumetric calculation of erosion rates. Secondly, the erosion rate derived from the delta sediments includes a lag associated with sediment transport through the catchment. The  $^{10}\text{Be}$  concentration is also affected by the sediment transport time, with longer times resulting in higher  $^{10}\text{Be}$  concentrations. Thus, any transient storage of sediments that were mobilized during the erosion pulse within the catchment would result in both a delay in the erosion signal in deposits at the catchment outlet, as well as decreased  $^{10}\text{Be}$ -derived erosion rates. However, based on satellite imagery and our helicopter reconnaissance, there do not appear to be any areas of significant storage apart from minor alluvial fans and fluvial terraces along the trunk stream.

Although each approach to estimating paleo-erosion rates suffers from limitations, the agreement of the estimates (within uncertainty) is encouraging. In general, we expect that the delta-volume estimates provide a robust minimum estimate of average erosion rates over the timespan of deposition. The  $^{10}\text{Be}$ -derived erosion-rate estimates may be broadly reasonable, but they are sensitive to changes in erosion processes that lead to non-uniform erosion (e.g., Niemi et al., 2005) and they may show significant lags when erosion rates change.

### 5.3. Landscape evolution derived from $^{10}\text{Be}$ data in the context of changing climate

Our modeling approach applied to the  $^{10}\text{Be}$  data illustrates that a 25 to 300-fold increase in erosion rates occurred at the onset of a wetter phase, at the upper-parts of the catchment, and that there were also likely changes in erosion processes to produce the very high erosion-rate outliers (BA-1 and BA-2). Theoretically, higher erosion rates in this environment could have been associated with a tectonically-created increase in relief or stream capture in the basement-rock sectors of the rift shoulders. However, there is neither evidence in support of such changes in the fluvial network, nor is there any depositional, morphologic, or structural evidence for accelerated faulting during the last 15 kyr (Melnick et al., 2012). Also, considering that the increased erosion rates occurred during a period of rising or high base level, we can rule out that the drainage network expanded following base-level fall. Assuming that the size of the Baragoi catchment, the morphologic characteristics, the exposure of quartz-bearing rocks, and tectonic activity have not changed significantly over the last 15 kyr, it is more likely that changes in climate and co-varying vegetation cover forced the changes in erosion rates.

The inferred increase in erosion rates at the beginning of the AHP is remarkable, given that paleo-Lake Suguta must have been characterized by a rising base level (Garcin et al., 2009; Junginger et al., 2014). We suggest that our high paleo-erosion rates resulted from an increase in precipitation and runoff on the scarcely vegetated, partly barren land surfaces during the last glacial period, when equatorial East Africa was relatively dry (Butzer et al., 1972; Gasse et al., 2008). Importantly, the  $^{10}\text{Be}$  data require not only a substantial increase in erosion rates during the lake-level rise, but also a sharp decrease in erosion rates when the lake level was still high. This short-lived erosional response to climatic forcing

has been predicted in numerical models, whereby increased runoff intensity triggers an expansion of the drainage network, removal of hillslope material, and a temporary increase in sediment supply to river channels (Tucker and Slingerland, 1997).

At first sight, higher erosion rates forced by a shift toward wetter conditions during the early AHP appears incompatible with a regional study of modern erosion rates in Kenya (Torres Acosta et al., 2015). These authors showed that for a given hillslope gradient, the highest erosion rates occur in regions characterized by low rainfall and intermediate vegetation cover, and lower rates characterized regions with a dense vegetation cover. Today, sparse vegetation cover, low rainfall, and low erosion rates characterize the Baragoi catchment. In this context, we hypothesize that regions with low rainfall and sparse vegetation are strongly impacted by erosion during the transition from dry to wet climate conditions. It can be envisaged that a shift toward more frequent rainfall on hillslopes would lead to faster erosion, while in river channels, it would lead to increased stream power, incision, and ensuing slope failures, causing higher sediment flux. Such a scenario is compatible with our interpretation of the  $^{10}\text{Be}$  data as reflecting non-uniform erosion processes and increased erosion rates at the onset of the wet period (see Section 4.4).

To reconcile this paleo-environmental scenario of greater erosivity with the present-day low erosion rates in the densely vegetated, humid sectors of the East African Rift (Torres Acosta et al., 2015), we propose that there must be a lag time in landscape response to climatic forcing. Accordingly, the early AHP changeover to wetter conditions initially forced an increase in erosion rates. This was superseded by a transition to environmental conditions where weathering and soil formation (e.g., Knox, 1972) provided the substrate for a denser, protective vegetation cover (e.g., Bull and Kirby, 2002), which in turn stabilized hillslopes and led to decreased erosion rates. No data on vegetation cover are available for the Suguta Valley during the AHP. However, in the South Basin of Lake Turkana, which is located 10 km to the north of the Suguta Valley, carbon isotopes of sedimentary leaf waxes indicate a mixed tree/grass vegetation from ~20 to ~13 cal. kyr BP, while trees ( $\text{C}_3$  plants) were ubiquitous during the AHP (Morrissey, 2014). Today, this arid basin mostly accommodates grasses ( $\text{C}_4$  plants). The hydrogen isotopes from the same leaf waxes suggest that the onset of increased precipitation occurred at ~14 cal. kyr BP and was abrupt, occurring over just centuries (Morrissey, 2014). Such large changes in vegetation and precipitation support our erosion-history scenario. Overall, our study adds to a growing body of model-based (e.g., Tucker and Slingerland, 1997; Istanbuluoglu and Bras, 2005), experimental (Loch, 2000), and field evidence (e.g., Vanacker et al., 2007; Molina et al., 2008; Torres Acosta et al., 2015) highlighting the importance of coupled climate variability and vegetation changes in controlling surface-process rates.

## 6. Conclusions

Cosmogenic  $^{10}\text{Be}$ -derived paleo- and modern catchment-mean erosion rates of fluvial-lacustrine sediments of the Baragoi catchment compared with reconstructed paleo-delta volume and lake levels document coupled changes in climate and erosion rates during the African Humid Period (AHP) in northern Kenya.  $^{10}\text{Be}$  concentrations derived from sands intercalated in the Baragoi paleo-delta show an increase in erosion rates during the early AHP, during a shift to wetter conditions. We suggest that initially, increased precipitation and runoff caused the formation of an approximately 300-m-deep lake and rapid hillslope erosion in the catchment areas, likely through processes that produced gullies and other types of deep hillslope excavation. To explain the subsequent decrease in erosion rates during the early Holocene when climate remained wet, we hypothesize that the protracted humid climate led to



faster soil production and the establishment of a denser vegetation cover, which helped stabilize the hillslopes and protect them from further rapid erosion. Hence, our observations suggest that the fastest erosion occurred during the lag time that likely existed between the onset of wetter conditions and the establishment of a denser vegetation cover. We conclude that climate variability is a principal factor modulating temporal variability of erosion rates in semi-arid regions, particularly in climatic threshold regions such as the dry sectors of equatorial East Africa.

## Acknowledgements

M.R.S. acknowledges funding through DFG (Deutsche Forschungsgemeinschaft) grant STR 373-18/1 and co-funding by grant TR419/6-3. V.T.A. was supported by the DFG Graduate School GRK1364 *Shaping Earth's Surface in a Variable Environment*, funded by DFG through a grant to M.R.S. (grant STR 373-20/1). We thank the Government of Kenya for research permits. Y.G. was supported by DFG grant GA 1629/2-2. T.F.S. was supported by the DFG's Emmy-Noether-Programme (grant SCHI 1241/1-1). D.M. was supported by DFG grant ME 3157/4-1. J.K.W. was supported by an Alexander von Humboldt postdoctoral fellowship. We thank S. Savi and L. Olaka for discussions and G. Sivri for help with sample preparation. We acknowledge the three anonymous referees who provided constructive and insightful comments.

## Appendix A. Supplementary material

Supplementary material related to this article can be found online at <http://dx.doi.org/10.1016/j.epsl.2016.11.017>.

## References

- Antinao, J.L., McDonald, E., 2013. A reduced relevance of vegetation change for alluvial aggradation in arid zones. *Geology* 41, 11–14.
- Baker, B.H., 1963. Geology of the Baragoi area. *Geol. Surv. Kenya, Nairobi* 53, 1–74.
- Balco, G., Stone, J.O., Lifton, N.A., Dunai, T.J., 2008. A complete and easily accessible means of calculating surface exposure ages or erosion rates from  $^{10}\text{Be}$  and  $^{26}\text{Al}$  measurements. *Quat. Geochronol.* 3, 174–195.
- BEICIP, Geological Map of Kenya, Ministry of Energy and Regional Development of Kenya, Rueil-Malmaison, France, 1987.
- Bergner, A.G.N., Strecker, M.R., Trauth, M.H., Deino, A., Gasse, F., Blisniuk, P., Duehnforth, M., 2009. Tectonic and climatic control on evolution of rift lakes in the Central Kenya Rift, East Africa. *Quat. Sci. Rev.* 28, 2804–2816.
- Bierman, P., Steig, E.J., 1996. Estimating rates of denudation using cosmogenic isotope abundances in sediment. *Earth Surf. Process. Landf.* 21, 125–139.
- Bronk Ramsey, C., 2001. Development of the radiocarbon calibration program OxCal. *Radiocarbon* 43, 355–363.
- Bull, L.J., Kirby, M.J., 2002. Dryland river characteristics and concepts. In: Bull, L.J., Kirby, M.J. (Eds.), *Dryland Rivers: Hydrology and Geomorphology of Semi-Arid Channels*, pp. 3–16.
- Butzer, K.W., Isaac, G.L., Richardson, J.L., Washbourn-Kamau, C., 1972. Radiocarbon dating of east African lake levels. *Science* 175, 1069–1076.
- Chmeleff, J., von Blanckenburg, F., Kossert, K., Jakob, D., 2010. Determination of the  $^{10}\text{Be}$  half-life by multicollector ICP-MS and liquid scintillation counting. *Nucl. Instrum. Methods B* 268, 192–199.
- deMenocal, P., Ortiz, J., Guilderson, T., Adkins, J., Sarnthein, M., Baker, L., Yarusinsky, M., 2000. Abrupt onset and termination of the African Humid Period: rapid climate responses to gradual insolation forcing. *Quat. Sci. Rev.* 19, 347–361.
- Dunkley, P.N., Smith, M., Allen, D.J., Darling, W.G., 1993. The Geothermal Activity and Geology of the Northern Sector of the Kenya Rift Valley. *British Geological Survey Research Report SC/93/1*. 185 pp.
- Enzel, Y., Amit, R., Grodek, T., Ayalon, A., Lekach, J., Porat, N., Bierman, P., Blum, J.D., Erel, Y., 2012. Late Quaternary weathering, erosion, and deposition in Nahal Yael, Israel: an “impact of climatic change on an arid watershed”? *Geol. Soc. Am. Bull.* 124, 705–722.
- Garcin, Y., Junginger, A., Melnick, D., Olago, D.O., Strecker, M.R., Trauth, M.H., 2009. Late Pleistocene–Holocene rise and collapse of Lake Suguta, northern Kenya Rift. *Quat. Sci. Rev.* 28, 911–925.
- Gasse, F., Chalié, F., Vincens, A., Williams, M.A.J., Williamson, D., 2008. Climatic patterns in equatorial and southern Africa from 30,000 to 10,000 years ago reconstructed from terrestrial and near-shore proxy data. *Quat. Sci. Rev.* 27, 2316–2340.
- Granger, D.E., Kirchner, J.W., Finkel, R., 1996. Spatially averaged long-term erosion rates measured from *in situ*-produced cosmogenic nuclides in alluvial sediment. *J. Geol.* 104, 249–257.
- Heimsath, A.M., Chappell, J., Fifield, K., 2010. Eroding Australia: rates and processes from Bega Valley to Arnhem Land. *Geol. Soc. (Lond.) Spec. Publ.* 346, 225–241.
- Istanbulluoglu, E., Bras, R.L., 2005. Vegetation-modulated landscape evolution: effects of vegetation on landscape processes, drainage density, and topography. *J. Geophys. Res., Earth Surf.* 110, F02012. <http://dx.doi.org/10.1029/2004JF000249>.
- Ivory, S.J., McGlue, M.M., Ellis, G.S., Lézine, A.-M., Cohen, A.S., Vincens, A., 2014. Vegetation controls on weathering intensity during the last deglacial transition in Southeast Africa. *PLoS ONE* 9, e112855. <http://dx.doi.org/10.1371/journal.pone.0112855>.
- Junginger, A., Roller, S., Olaka, L.A., Trauth, M.H., 2014. The effects of solar irradiation changes on the migration of the Congo Air Boundary and water levels of paleo-Lake Suguta, Northern Kenya Rift, during the African Humid Period (15–5 ka BP). *Palaeogeogr. Palaeoclimatol. Palaeoecol.* 396, 1–16.
- Kendall, R.L., 1969. An ecological history of the Lake Victoria basin. *Ecol. Monogr.* 39, 121–176.
- Knox, J.C., 1972. Valley alluviation in southwestern Wisconsin. *Ann. Assoc. Am. Geogr.* 62, 401–410.
- Kohl, C.P., Nishiizumi, K., 1992. Chemical isolation of quartz for measurement of *in situ*-produced cosmogenic nuclides. *Geochim. Cosmochim. Acta* 56, 3583–3587.
- Korschinek, G., Bergmaier, A., Faestermann, T., Gerstmann, U.C., Knie, K., Rugel, G., Wallner, A., Dillmann, I., Dollinger, G., von Gostomski, C.L., Kossert, K., Maiti, M., Poutivtsev, M., Remmert, A., 2010. A new value for the half-life of  $^{10}\text{Be}$  by heavy-ion elastic recoil detection and liquid scintillation counting. *Nucl. Instrum. Methods B* 268, 187–191.
- Lague, D., Hovius, N., Davy, P., 2005. Discharge, discharge variability, and the bedrock channel profile. *J. Geophys. Res.* 110, F04006. <http://dx.doi.org/10.1029/2004JF000259>.
- Lal, D., 1991. Cosmic ray labeling of erosion surfaces: *in situ* nuclide production rates and erosion models. *Earth Planet. Sci. Lett.* 104, 424–439.
- Loch, R.J., 2000. Effects of vegetation cover on runoff and erosion under simulated rain and overland flow on a rehabilitated site on the Meandu Mine, Tarong, Queensland. *Aust. J. Soil Res.* 38, 299–312.
- Melnick, D., Garcin, Y., Quinteros, J., Strecker, M.R., Olago, D., Tiercelin, J.-J., 2012. Steady rifting in northern Kenya inferred from deformed Holocene lake shorelines of the Suguta and Turkana basins. *Earth Planet. Sci. Lett.* 331–332, 335–346.
- Molina, A., Govers, G., Poesen, J., Van Hemelryck, H., De Bievre, B., Vanacker, V., 2008. Environmental factors controlling spatial variation in sediment yield in a central Andean mountain area. *Geomorphology* 98, 176–186.
- Morrissey, A., 2014. Stratigraphic Framework and Quaternary Paleolimnology of the Lake Turkana Rift, Kenya. PhD dissertation, Syracuse University, NY, USA. 188 pp.
- Morrissey, A., Scholz, C.A., 2014. Paleohydrology of Lake Turkana and its influence on the Nile River system. *Palaeogeogr. Palaeoclimatol. Palaeoecol.* 403, 88–100.
- Nicholson, S.E., 1996. A review of climate dynamics and climate variability in eastern Africa. In: Johnson, T.C., Odada, E.O. (Eds.), *The Limnology, Climatology and Paleoclimatology of the East African Lakes*. Gordon and Breach Publishers, Amsterdam, pp. 25–56.
- Niemi, N.A., Oskin, M., Burbank, D.W., Heimsath, A.M., Gabet, E.J., 2005. Effects of bedrock landslides on cosmogenically determined erosion rates. *Earth Planet. Sci. Lett.* 237, 480–498.
- Ojany, F.F., Ogenoo, R.B., 1973. Kenya: A Study in Physical and Human Geography. Longman, Nairobi. 228 pp.
- Pelletier, J.D., Brad Murray, A., Pierce, J.L., Bierman, P.R., Breshears, D.D., Crosby, B.T., Ellis, M., Foufoula-Georgiou, E., Heimsath, A.M., Houser, C., Lancaster, N., Marani, M., Merritts, D.J., Moore, L.J., Pederson, J.L., Poulos, M.J., Rittenour, T.M., Rowland, J.C., Ruggiero, P., Ward, D.J., Wickert, A.D., Yager, E.M., 2015. Forecasting the response of Earth's surface to future climatic and land use changes: a review of methods and research needs. *Earth's Future* 3. <http://dx.doi.org/10.1002/2014EF000290>.
- Reimer, P.J., Bard, E., Bayliss, A., Beck, J.W., Blackwell, P.G., Bronk Ramsey, C., Buck, C.E., Cheng, H., Edwards, R.L., Friedrich, M., Grootes, P.M., Guilderson, T.P., Haffidason, H., Hajdas, I., Hatté, C., Heath, T.J., Hoffmann, D.L., Hogg, A.G., Hughen, K.A., Kaiser, K.F., Kromer, B., Manning, S.W., Niu, M., Reimer, R.W., Richards, D.A., Scott, E.M., Southon, J.R., Staff, R.A., Turney, C.S.M., van der Plicht, J., 2013. IntCal13 and Marine13 Radiocarbon Age Calibration Curves 0–50,000 Years cal BP. *Radiocarbon* 55, 1869–1887.
- Richardson, J.L., Dussinger, R.A., 1986. Paleolimnology of mid-elevation lakes in the Kenya Rift Valley. *Hydrobiologia* 143, 167–174.
- Schaller, M., von Blanckenburg, F., Veldkamp, A., Tebbens, L.A., Hovius, N., Kubik, P.W., 2002. A 30,000 yr record of erosion rates from cosmogenic  $^{10}\text{Be}$  in Middle European river terraces. *Earth Planet. Sci. Lett.* 204, 307–320.
- Schildgen, T.F., Robinson, R.A.J., Savi, S., Phillips, W.M., Spencer, J.Q.G., Bookhagen, B., Scherler, D., Tofelde, S., Alonso, R.N., Kubik, P.W., Binnie, S.A., Strecker, M.R., 2016. Landscape response to late Pleistocene climate change in NW Argentina: sediment flux modulated by basin geometry and connectivity. *J. Geophys. Res., Earth Surf.* 121, 392–414.

- Schumm, S.A., 1993. River response to baselevel change: implications for sequence stratigraphy. *J. Geol.* 101, 279–294.
- Shanahan, T.M., McKay, N.P., Hughen, K.A., Overpeck, J.T., Otto-Bliesner, B., Heil, C.W., King, J., Scholz, C.A., Peck, J., 2015. The time-transgressive termination of the African Humid Period. *Nat. Geosci.* 8, 140–144.
- Summerfield, M.A., Hulton, N.J., 1994. Natural controls of fluvial denudation rates in major world drainage basins. *J. Geophys. Res.* 99, 13871–13883.
- Tierney, J.E., Russell, J.M., Huang, Y., 2010. A molecular perspective on Late Quaternary climate and vegetation change in the Lake Tanganyika basin, East Africa. *Quat. Sci. Rev.* 29, 787–800.
- Torres Acosta, V., Schildgen, T.F., Clarke, B.A., Scherler, D., Bookhagen, B., Wittmann, H., von Blanckenburg, F., Strecker, M.R., 2015. Effect of vegetation cover on millennial-scale landscape denudation rates in East Africa. *Lithosphere* 7, 408–420.
- Truckle, P.H., 1976. Geology and late Cainozoic lake sediments of Suguta Trough, Kenya. *Nature* 263, 380–383.
- Tucker, G.E., Slingerland, R., 1997. Drainage basin responses to climate change. *Water Resour. Res.* 33, 2031–2047.
- Vanacker, V., von Blanckenburg, F., Govers, G., Molina, A., Poesen, J., Deckers, J., Kubik, P., 2007. Restoring dense vegetation can slow mountain erosion to near natural benchmark levels. *Geology* 35, 303–306.
- von Blanckenburg, F., Hewawasam, T., Kubik, P.W., 2004. Cosmogenic nuclide evidence for low weathering and denudation in the wet, tropical highlands of Sri Lanka. *J. Geophys. Res., Earth Surf.* 109, F03008. <http://dx.doi.org/10.1029/2003JF000049>.
- von Blanckenburg, F., 2005. The control mechanisms of erosion and weathering at basin scale from cosmogenic nuclides in river sediment. *Earth Planet. Sci. Lett.* 237, 462–479.
- Wolff, C., Haug, G.H., Timmermann, A., Sinninghe Damsté, J.S., Brauer, A., Sigman, D.M., Cane, M.A., Verschuren, D., 2011. Reduced interannual rainfall variability in east Africa during the last ice age. *Science* 333, 743–747.